Applied Catalysis B: Environmental 297 (2021) 120446

Contents lists available at ScienceDirect

Applied Catalysis B: Environmental

journal homepage: www.elsevier.com/locate/apcatb

Biomass-derived pyrolytic carbons accelerated Fe(III)/Fe(II) redox cycle for persulfate activation: Pyrolysis temperature-depended performance and mechanisms

Jun Liang [a], Xiaoguang Duan [b], Xiaoyun Xu [a,*], Kexin Chen [a], Fei Wu [c], Hao Qiu [a], Chengshuai Liu [c], Shaobin Wang [b], Xinde Cao [a,d]

[a] School of Environmental Science and Engineering, Shanghai Jiao Tong University, Shanghai, 200240, China
[b] School of Chemical Engineering and Advanced Materials, The University of Adelaide, Adelaide, SA5005, Australia
[c] State Key Laboratory of Environmental Geochemistry, Institute of Geochemistry, Chinese Academy of Sciences, Guiyang, 550081, China
[d] Shanghai Institute of Pollution Control and Ecological Security, Shanghai, 200092, China

ARTICLE INFO

Keywords:
Pyrolytic carbon
Persulfate
Fe(III)/Fe(II) cycle
Fe(IV)
Electron transfer

ABSTRACT

The oxidation efficiency of iron/persulfate coupled system was limited by the sluggish Fe^{3+}/Fe^{2+} cycle and severe Fe^{3+} precipitation. In this study, we reported that pyrolytic carbon under low-temperature (PC400) could significantly and continuously accelerate the Fe^{3+}/Fe^{2+} circulation in the Fe^{3+}-mediated persulfate system. The fast Fe^{3+}/Fe^{2+} circulation was due to the transformation between semiquinone radicals and quinones on PC400, resulting in the great reusability and continuous degradation of sulfamethoxazole (SMX). In contrast, pyrolytic carbon derived under high temperature (PC700) could not maintain the Fe^{3+}/Fe^{2+} cycle for continuous SMX degradation. SMX removal in both two systems was barely affected by the presence of chloride and humic acid. Even in the real water matrixes (e.g., seawater, piggery wastewater, and landfill leachate), appreciable SMX removal was obtained because of the nonradical reaction pathways, including high-valence Fe(IV) and surface electron-transfer process, verified by methyl phenyl sulfoxide-based probe tests, Mössbauer spectroscopy, electrochemical test, and kinetic calculation. This study advances the knowledge of Fe^{3+}-mediated persulfate reaction enhanced by pyrolytic carbons. The outcomes will inspire new strategies for developing cost-effective and efficient carbon-accelerated Fenton-like systems.

1. Introduction

Classic Fenton reactions use Fe^{2+} and hydrogen peroxide to generate hydroxyl radicals (•OH) to eliminate organic pollutants in water [1]. Compared to •OH, the longer lifetime and higher redox potential of sulfate radicals ($SO_4^{\bullet-}$) enables more efficient degradation of pollutants in the Fe^{2+} and persulfate (PS) coupled system [2,3]. One mole of Fe^{2+} produces one mole of sulfate radical in the Fe^{2+}/PS system (Eq. (1)). However, the regeneration rate of Fe^{2+} (Eq. (2)) is much lower than the consumption rate (Eq. (1)) [4,5]. Therefore, Fe^{2+} regeneration from Fe^{3+} is the rate-determining step in the Fe^{2+}/PS system.

$$Fe^{2+} + S_2O_8^{2-} \rightarrow Fe^{3+} + SO_4^{\bullet-} + SO_4^{2-} \quad (1)$$

$$Fe^{3+} + S_2O_8^{2-} \rightarrow Fe^{2+} + S_2O_8^{\bullet-} \quad (2)$$

Considerable efforts have been undertaken to accelerate the Fe^{2+}/Fe^{3+} circulation. Reductive agents and iron chelating agents are the typical promotors for Fe^{3+} reduction [6–13]. Reductive agents (e.g., hydroxylamine and ascorbic acid) can directly reduce Fe^{3+} to Fe^{2+}, herein facilitating the reaction between Fe^{2+} and PS [6–8,14]. Iron chelating agents (e.g., citric acid and ethylenediaminetetraacetate (EDTA)) have been used to increase the concentration of dissolved iron species and tune the redox potential of iron-chelator complexes to accelerate the cycling of Fe^{2+}/Fe^{3+} [11,15]. However, these chemical reagents might induce secondary pollution and compete with the target pollutants to consume the reactive oxygen species (ROS) [16].

Carbonaceous materials are promising alternatives to these reductive agents because carbons can effectively reduce Fe^{3+} without energy input or extra addition of toxic chemicals [9,17,18]. Some researchers indicated that the formed carbon-Fe^{3+} complexes (e.g., fullerene-Fe^{3+} and

* Corresponding author.
E-mail address: xuxiaoyun@sjtu.edu.cn (X. Xu).

https://doi.org/10.1016/j.apcatb.2021.120446
Received 5 April 2021; Received in revised form 1 June 2021; Accepted 10 June 2021
Available online 15 June 2021

carbon nanotube-Fe^{3+} complexes) possessed more active Fe^{3+} species with a high oxidative potential, which could accelerate the Fe^{3+}/Fe^{2+} redox cycles and enhance the pollutants degradation [19,20]. We previously reported that pyrolytic carbons (PC) produced from biomass waste could act as both "electron donor" to reduce pollutants and "electron shuttle" to mediate the reduction of pollutants by lactate [21]. The redox characteristics of pyrolytic carbons were related to the persistent free radicals (PFR) [22], surface functional groups (i.e. phenolic O-H and quinones) [21], and conjugated structure [23–25]. Therefore, pyrolytic carbons are promising and cost-effective catalysts to accelerate the Fe^{3+}/Fe^{2+} cycle through redox reactions. Surface electron transfer was hypothesized to be the possible reaction pathway, i.e., electron migrates from the electron-donor of pollutant to the acceptor of reactive carbons/PS complexes through the conductive bridge of pyrolytic carbons [26]. Besides, previous study reported that Fe^{2+} could react with PS to generate Fe(IV) [27,28]. However, similar nonradical pathways mediated by carbons were rarely reported and the dominant reactive species were still ambiguous.

Herein, the aim of this study was to investigate the catalytic performance and elucidate the mechanism of the PC/Fe^{3+}/PS system. The conversion of Fe^{3+}/Fe^{2+} was detected and verified by specific chelating agents. The reactive species were determined via diverse methods including quenching experiment, electron paramagnetic resonance (EPR), methyl phenyl sulfoxide (PMSO) probing test, Mössbauer spectroscopy, electrochemical test, and kinetic calculation. The reusability and stability of pyrolytic carbon was also evaluated. More importantly, this oxidative system was applied in real water matrixes including lake water, seawater, piggery wastewater, and landfill leachate.

2. Materials and methods

2.1. Materials and experimental reagents

Materials and experimental reagents were provided in Text S1 of the supporting materials.

2.2. Preparation of pyrolytic carbon

The approach for the preparation of pyrolytic carbons derived from peanut shell was based on our previous studies [21,29]. Peanut shell was adopted as the carbon precursor due to its high lignin content and less ash impurities [30]. The peanut shell was pyrolyzed at 400 °C and 700 °C under N_2 atmosphere for 4 h, which were denoted as PC400 and PC700, respectively. These two temperatures were selected because the resulted pyrolytic carbons showed the different catalytic performance and mechanisms for the SMX degradation according to our previous study [31]. The resulted pyrolytic carbon was ground by a ball mill (QM-3SP04, China), and then passed through a 100-mesh sieve. Characterization methodologies for the as-prepared materials were described in Text S2, and the characterization results are shown in Table S1 in the supporting materials.

2.3. Catalytic degradation experiment

The catalytic experiments were performed in the 100-mL bottle with the mixture of pyrolytic carbon (0.5 g L^{-1}), Fe^{3+} (1 mmol L^{-1}), PS (2 mmol L^{-1}), and SMX (10 mg L^{-1}). Graphite was used for the comparison. The solution pH was adjusted to 3.5 by diluted solutions of hydrochloric acid and sodium hydroxide before reaction. At given time intervals, 0.5 mL samples were collected and mixed with 0.5 mL methanol, and then filtered through a membrane (0.45-μm). The concentration of SMX was quantified by a high-performance liquid chromatography (HPLC, Waters, 2489, USA). The same procedure as described above was also conducted for identifying the free radicals on EPR (Micro EPR, Bruker, Germany), using DMPO as the trapping agent.

Effect of experimental factors containing pH (3.5/7/9/11), Cl^- (10 mmol L^{-1}), and humic acid (1 and 10 mg L^{-1}) was investigated. For reusability tests, the pyrolytic carbon was reused 5 times. After every cycle, pyrolytic carbon was collected through centrifugation, water washed, and the used pyrolytic carbons was added in the successive cycles. For continuous catalytic tests, pyrolytic carbon and Fe^{3+} was only added in the first run, while PS and SMX were added for successively three runs.

Table 1
Characteristics of the real water samples.

Parameters	Lake water	Seawater	Piggery wastewater	Landfill leachate
TOC (mg L^{-1})	9.2	9.3	821	1389
Conductivity (μS)	480	17280	6870	20200
F^- (mg L^{-1})	1.6	–	0.081	2.7
Cl^- (mg L^{-1})	80.2	7286	418.1	4479
Br^- (mg L^{-1})	1.8	–	24.67	46.8
NO_3^- (mg L^{-1})	2.7	–	1.63	3.12
NO_2^- (mg L^{-1})	–	–	9.58	71.3
SO_4^{2-} (mg L^{-1})	38.5	1097	39.9	129.5
SMX (mg L^{-1})	–	0.021	0.08	–

2.4. Analysis of reactive species

2.4.1. Radical quenching tests

Radical quenching tests were performed to identify the dominant reactive species in the PC/Fe^{3+}/PS system using the quenchers (e.g., ethanol, furfuryl alcohol (FFA), and phenol). Ethanol could quench the free radicals [32]. FFA was used as quencher for singlet oxygen ($^1O_2$) [17]. In comparison, phenol could quench both the radical and nonradical reactive species (e.g., high-valence Fe(IV) and surface-confined electron transfer) [28].

2.4.2. Identification of nonradical species

To identify the possible surface electron-transfer, Linear Sweep Voltammetry (LSV) measurements were performed using the three-electrode cell according to the reported methods [33]. The detailed procedure and parameters of LSV measurements were described in Text S3 in the supporting materials.

To identify the Fe(IV) species, PMSO was used as the specific chemical probe in the PC/Fe^{3+}/PS system by detecting the concentrations of PMSO and the characteristic product, methyl phenyl sulfone ($PMSO_2$), because PMSO could be oxidized by Fe(IV) to generate $PMSO_2$ [27]. To further verify the existing Fe(IV), Mössbauer experiment was conducted based on the reported method [34]. Briefly, the withdrawn sample was immediately added to the customized PTFE container and rapidly freeze-dried using liquid nitrogen. Then, sample was packed into a Delrin Mössbauer cup. The spectra were collected at 14 K in a transmission mode. The Mössbauer spectra of sample were measured by an automated precision Mössbauer spectrometric system with a high-velocity resolution (registration in 1024 channels) built based on a Mössbauer spectrometer (WSS-10, WissEl GmbH, Germany).

2.5. Application in the real water matrixes

Real water samples including lake water, seawater, piggery wastewater, and landfill leachate, were collected from the Siyuan lake, East China Sea, a pig farm, and a waste landfill, respectively, located in Shanghai. The water samples were filtered with a 0.45 μm mixed cellulose ester membrane and then stored at 4 °C before use. The characteristics of water samples were analyzed and displayed in Table 1. The two different PC/Fe^{3+}/PS systems were applied in the above real water systems. The experimental procedure was performed as described in section 2.3.

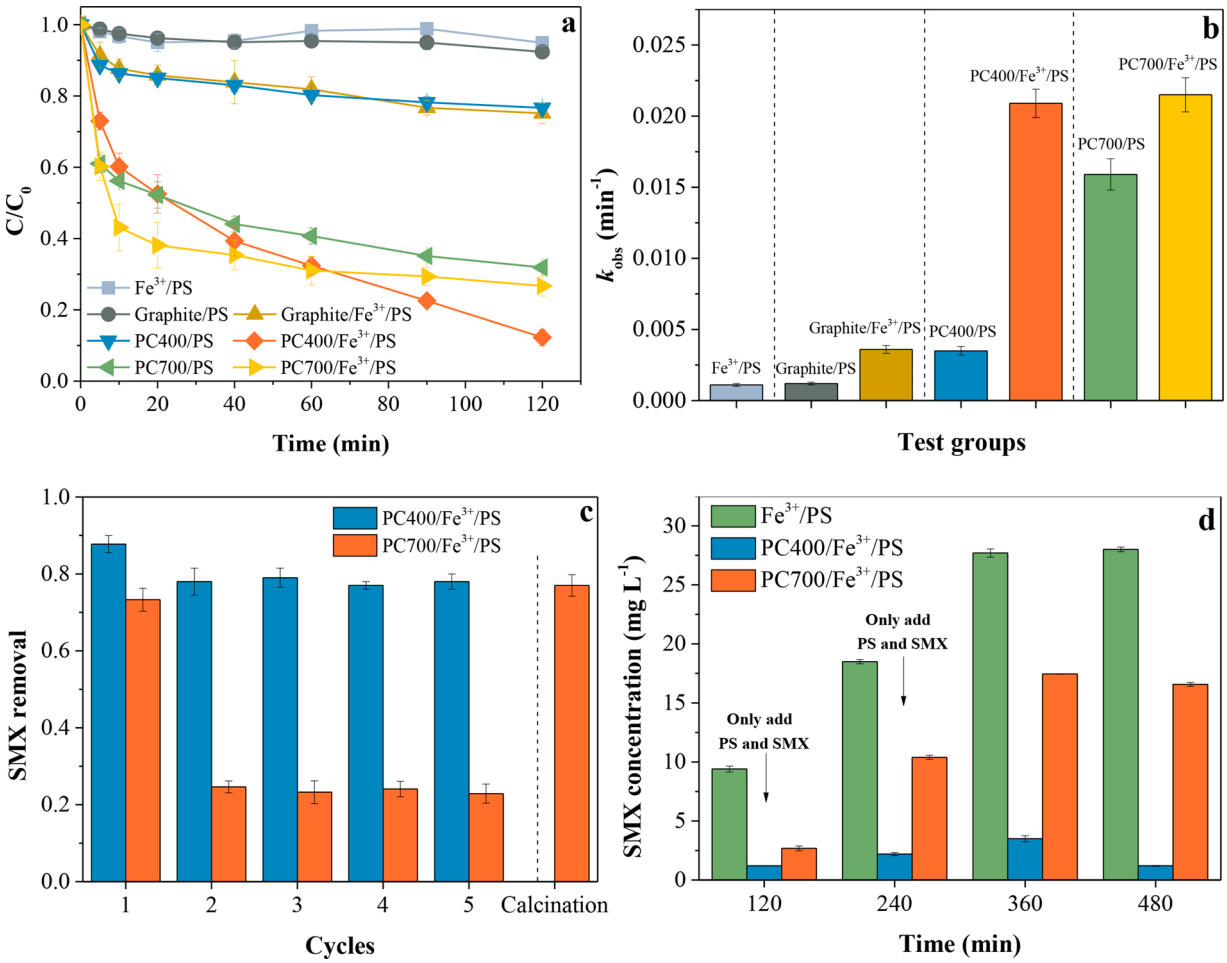

Fig. 1. SMX removal in different systems (a); k_{obs} of SMX removal in different systems (b); catalytic property of pyrolytic carbon for repeated use (c); continuous degradation of SMX in the Fe^{3+}/PS, PC400/Fe^{3+}/PS and PC700/Fe^{3+}/PS systems (d). Reaction conditions: PS: 2 mmol L^{-1}, Fe^{3+}: 1 mmol L^{-1}, pH = 3.5, and temperature: 25 °C (a-b) SMX: 10 mg L^{-1}, Graphite or PC400 or PC700: 0.5 g L^{-1}; (c) PC400 or PC700: 0.5 g L^{-1}, SMX: 10 mg L^{-1}; (d) SMX: totally 30 mg L^{-1}.

2.6. Analysis methods

The concentrations of SMX, PMSO, and $PMSO_2$ were quantified using HPLC. The SMX degradation products were analyzed by UHPLC-MS. The concentration of Fe^{2+} and total Fe were measured by the addition of 1,10-phenanthroline method with the absence and presence of hydroxylamine hydrochloride, respectively [35]. The detailed measuring methods of UHPLC-MS and Fe analysis were presented in Text S4. The total organic carbon (TOC) content was measured by a TOC analyzer (TOC-V, Shimadzu, Japan). The ionic composition was determined by an ionic chromatographic analyzer (ICS-5000, Thermo Fisher).

3. Results and discussion

3.1. Catalytic removal of SMX in different systems

SMX removal in both Fe^{3+}/PS and graphite/PS systems was ineffective (<7.65 %) (Fig. 1a). The addition of graphite enhanced SMX removal to 24.9 % in graphite/Fe^{3+}/PS system. Impressively, PC400 addition enhanced the SMX removal to 87.7 % in the PC400/Fe^{3+}/PS system, while only 23.3 % of SMX removal was observed in the PC400/PS system (Fig. 1a). SMX removal in the PC400/Fe^{3+}/PS system after 60 min was even higher than that in the classical Fe^{2+}/PS system (Fig. S1). In comparison, SMX removal in the PC700/Fe^{3+}/PS system was 73.3 %, while the PC700/PS system removed 68.1 % of SMX, indicating that the coupled PC700/PS might dominate the SMX removal in the PC700/Fe^{3+}/PS system (Fig. 1a). The removal of SMX in the Fe^{3+}/PS system assisted by graphite and pyrolytic carbon could be attributed to the degradation since SMX sorption by these materials was relatively limited (3.22 %–19.9 %) (Fig. S2). Both PC400/Fe^{3+}/PS and PC700/Fe^{3+}/PS system experienced two stages in the SMX removal, a rapid "first stage" and slow "second stage". Compared to that in the PC700/Fe^{3+}/PS system, the much faster removal of SMX in the second stage in the PC400/Fe^{3+}/PS system was likely to be induced by the fast generation of Fe^{2+}, which was detailedly presented in Section 3.2. Moreover, though the first-order rate constant (k_{obs}) in the graphite/Fe^{3+}/PS system (0.0036 min^{-1}) was 3 times of the graphite/PS system (0.0012 min^{-1}), the value of graphite/Fe^{3+}/PS system was still much lower than that of the PC400/Fe^{3+}/PS (0.0209 min^{-1}) and PC700/Fe^{3+}/PS system (0.0215 min^{-1}) (Fig. 1b). The catalytic activity of graphite was weaker than that of pyrolytic carbons, which might be ascribed to the much lower electron donating capability (0.075 vs 0.39–1.25 mmol e- (g carbon)$^{-1}$, Table S1) and sorption ability (Fig S2). The k_{obs} value of the PC400/Fe^{3+}/PS system was 4.97 times higher than that of the PC400/PS system, while k_{obs} of the PC700/Fe^{3+}/PS system was 1.35-time of the PC700/PS system. These results suggested that compared to PC700, PC400 might induce more Fe^{3+} reduction for PS activation and thereby accelerating the SMX degradation.

The reusability tests of the pyrolytic carbons were evaluated upon five successive cycles (Fig. 1c). In the PC400/Fe^{3+}/PS system, 78.0 % of SMX degradation was still observed after five cycles, which was slightly lower than the first run (87.7 %). However, in the PC700/Fe^{3+}/PS system, only 24.7 % of SMX degradation was obtained after the 2nd runs, and it kept constant in the following runs compared to 73.3 % of

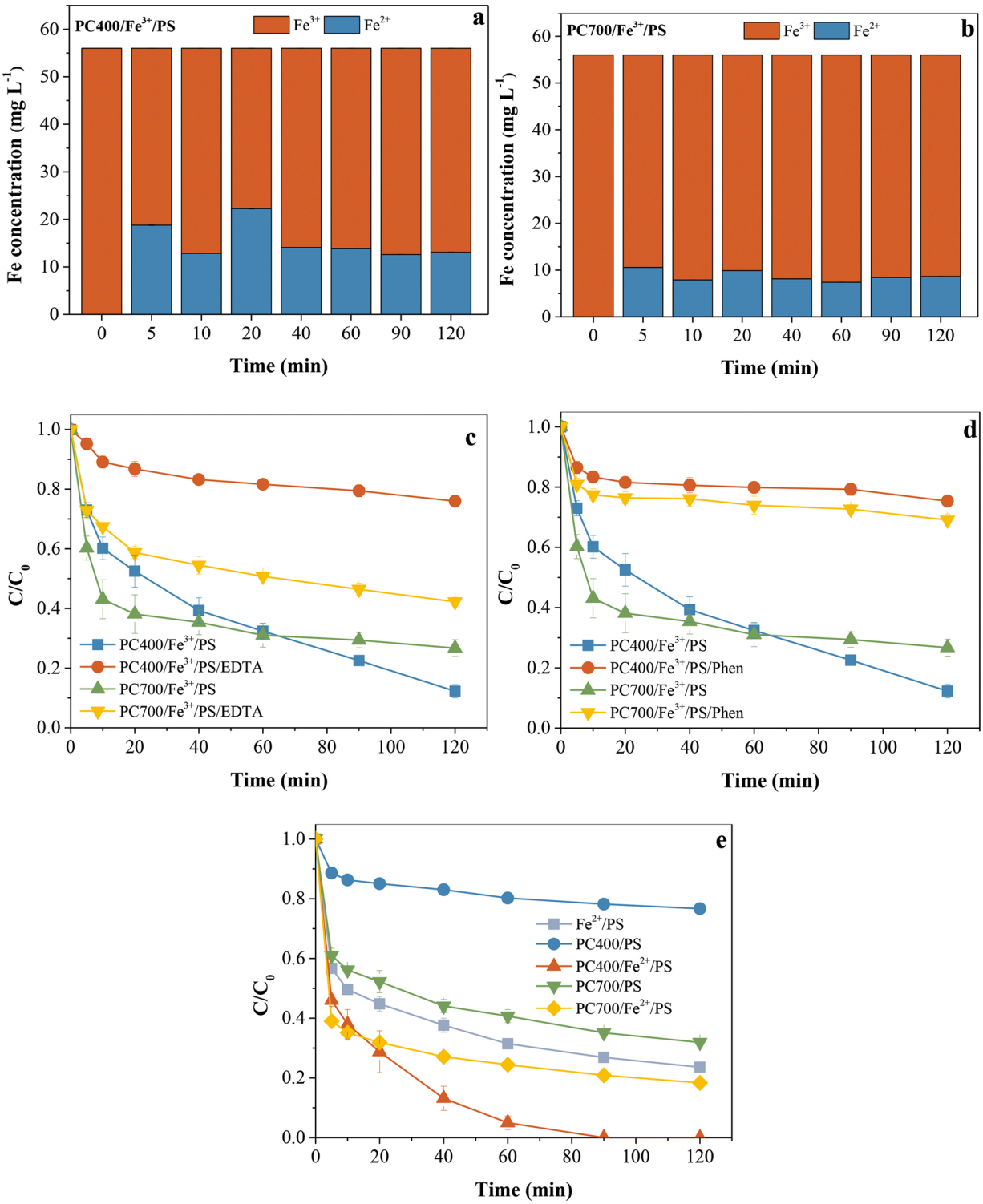

Fig. 2. Transformation of iron species (e.g., total Fe^{2+} and Fe^{3+}) in PC400/Fe^{3+}/PS (a) and PC700/Fe^{3+}/PS systems (b); the effect of EDTA (c) and Phen (d) on SMX removal in different systems; SMX removal in different Fe^{2+}-based systems (e). Reaction conditions: SMX: 10 mg L^{-1}, PS: 2 mmol L^{-1}, PC400/PC700: 0.5 g L^{-1}, pH = 3.5, (a-b) Fe^{3+}: 1 mmol L^{-1}; (c) EDTA: 1 mmol L^{-1}, Fe^{3+}: 1 mmol L^{-1}; (d) Phen: 1 mmol L^{-1}, Fe^{3+}: 1 mmol L^{-1}; (e) Fe^{2+}: 1 mmol L^{-1}.

degradation by the fresh PC700/Fe^{3+}/PS system (Fig. 1c). Meanwhile, in the PC700/PS system, after the 2nd runs, only 25.1 % of SMX removal was obtained although 68.1 % of SMX removal was observed after the 1nd cycle, and it kept constant in the following runs (Fig. S3). These results demonstrated that the deactivation of PC700/Fe^{3+}/PS was mainly caused by PC700 rather than Fe ions. It seemed that PC400 would recover its catalytic ability in the PC400/Fe^{3+}/PS system, and the reason for this was discussed in Section 3.4. However, PC700 was liable to be deactivated after use. Previous research attributed the deactivation to the block of pores and coverage of active sites [36]. The catalytic ability of PC700 was recovered in the PC700/Fe^{3+}/PS system by thermal treatment (700 °C, N_2 atmosphere), further proving the above explanation (Fig. 1c). Moreover, the continuous catalytic activity of pyrolytic carbon was evaluated in the PC400/Fe^{3+}/PS and PC700/Fe^{3+}/PS

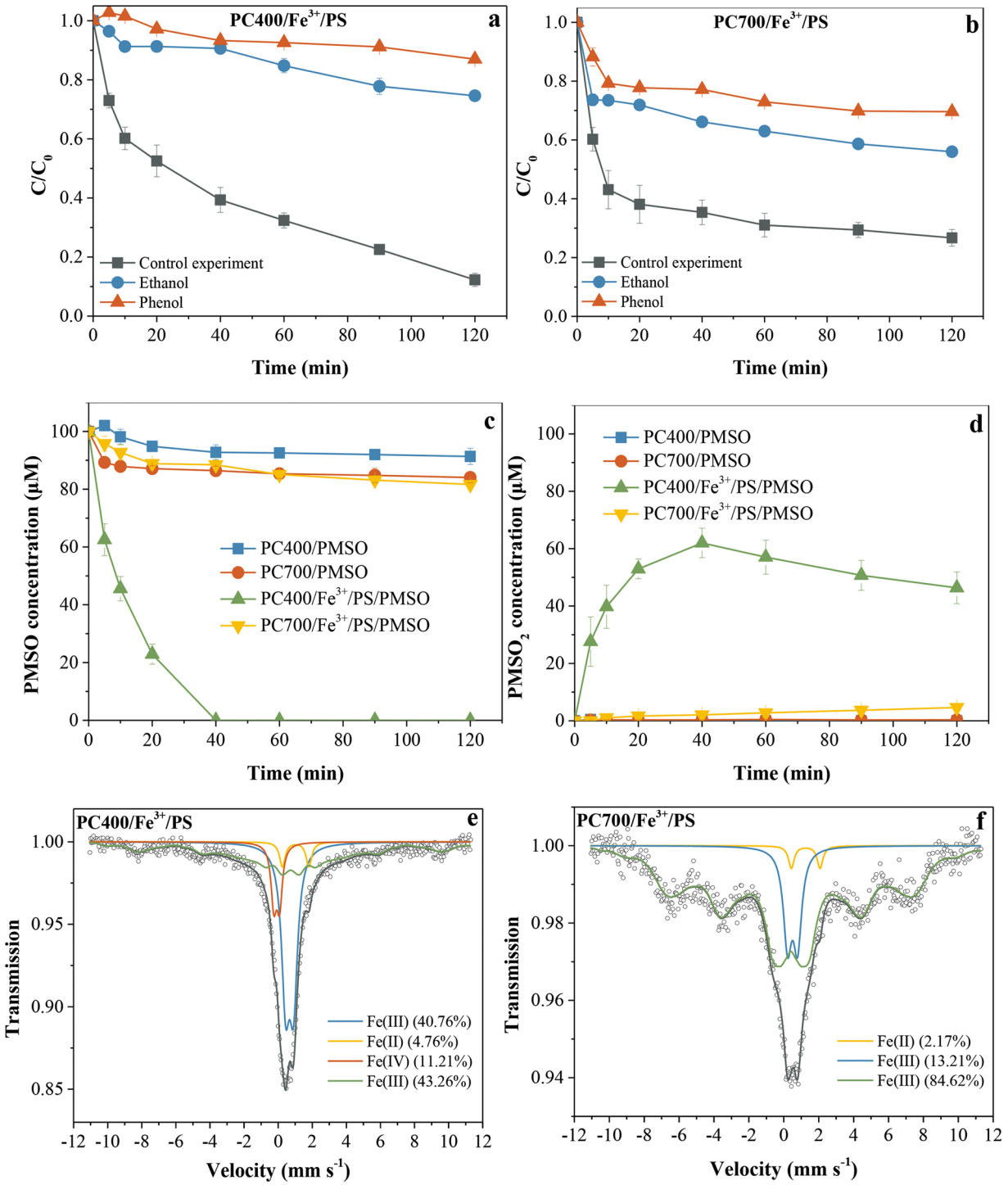

Fig. 3. Influence of different quenchers on SMX removal in the PC400/Fe^{3+}/PS (a) and PC700/Fe^{3+}/PS (b) systems; PMSO depletion (c) and $PMSO_2$ generation (d) in different systems; Mössbauer spectra of PC400/$^{57}Fe^{3+}$/PS (e) and PC700/$^{57}Fe^{3+}$/PS (f) systems. The spectra were collected at 14 K in transmission mode. Reaction conditions: (a-b) SMX: 10 mg L^{-1}, PS: 2 mmol L^{-1}, PC400/PC700: 0.5 g L^{-1}, Fe^{3+}: 1 mmol L^{-1}, Ethanol: 2 mol L^{-1}, Phenol: 0.04 mol L^{-1}, pH = 3.5; (c-d) PS: 2 mmol L^{-1}, PC400 or PC700: 0.5 g L^{-1}, Fe^{3+}: 1 mmol L^{-1}, PMSO: 100 μmol L^{-1}, and pH = 3.5; (e-f) PC400 or PC700: 5 g L^{-1}, $^{57}Fe^{3+}$: 10 mmol L^{-1}, PS: 20 mmol L^{-1}, and pH = 3.5.

systems (Fig. 1d). SMX concentration in the Fe^{3+}/PS system continuously increased with three runs of SMX addition and reached 28.0 mg L^{-1} at 480 min. However, SMX concentration in the PC400/Fe^{3+}/PS system was 1.20 mg L^{-1} after 480-min reaction, which was much lower than that of 16.6 mg L^{-1} SMX in the PC700/Fe^{3+}/PS system. The results further indicated that, compared to PC700, PC400 might be more liable to facilitate the Fe^{2+}/Fe^{3+} circulation, thus accelerating the formation of reactive species for continuous SMX degradation [12].

3.2. *Acceleration of Fe^{3+}/Fe^{2+} conversion*

The SEM images proved that unlike graphite (Fig. S4), Fe and C coexisted in pyrolytic carbon, which was uniformly distributed on the surface of pyrolytic carbon (Fig. S5), suggesting the potential interaction

between pyrolytic carbon and Fe^{3+}. In the graphite/Fe^{3+}/PS system, the concentration of Fe^{2+} was below detection limit (Fig. S6). In the PC400/Fe^{3+}/PS system, the concentrations of Fe^{2+} and Fe^{3+} were in a dynamic cycle for 40 min, and then maintained constant (Fig. 2a). The concentration of Fe^{2+} ranged from 12.6–22.3 mg L^{-1}. However, in the PC700/Fe^{3+}/PS system, the Fe^{3+}/Fe^{2+} cycle was much slower than that of PC400/Fe^{3+}/PS system, and concentration of Fe^{2+} varied from 7.91 to 10.6 mg L^{-1} (Fig. 2b). Note that the concentration of dissolved Fe^{2+} in both PC400/Fe^{3+}/PS and PC700/Fe^{3+}/PS systems was very low (<3.46 mg L^{-1}) (Fig. S7). In contrast, Fe^{2+} in the solid phase was significant, especially in the PC400/Fe^{3+}/PS system (9.41–21.0 mg L^{-1}), which suggested that surface-associated Fe^{2+} might be responsible for the surface Fe^{3+}/Fe^{2+} cycle in PC400/Fe^{3+}/PS. These results indicated that PC400 possessed a greater ability than PC700 for continuously reducing Fe^{3+} to Fe^{2+}.

To confirm the dynamic cycle of Fe^{2+} and Fe^{3+}, EDTA and Phen was employed to compete for the Fe species with pyrolytic carbon, respectively. Previous study reported that Fe^{3+}-EDTA complex was more stable than Fe^{2+}-EDTA complex; Fe^{2+}-Phen complex was more stable than Fe^{3+}-Phen complex [37]. Both EDTA and Phen addition significantly inhibited SMX removal (>63.7 %) in the PC400/Fe^{3+}/PS system (Fig. 2c-d) due to the hindered conversion between Fe^{2+} and Fe^{3+}, which further demonstrated the vital roles of the dynamic cycle between Fe^{2+} and Fe^{3+}. In the PC700/Fe^{3+}/PS system, Phen remarkably inhibited the SMX removal by 42.4 %; however, the reduction of SMX removal was relatively limited (15.5 %) with the addition of EDTA (Fig. 2c-d). This might be due to the different electric charge states of $[Fe(EDTA)]^-$ and $[Fe(Phen)_3]^{2+}$ [38], which affected the interactions between PC700 and PS. Compared to $[Fe(EDTA)]^-$, $[Fe(Phen)_3]^{2+}$ was more liable to be sorbed by the negatively-charged PC700 (Fig. S8), inducing more suppression of the SMX degradation in the PC700/Fe^{3+}/PS system. Although Fe^{3+} coordinated by EDTA might promote PS activation, the reducing ability of Fe^{3+}-EDTA complex was lower than that of Fe^{2+} [39], so here EDTA resulted in more inhibition of SMX degradation. Besides, EDTA addition had negligible roles on the SMX removal in the PC400/PS and PC700/PS system (Fig. S9), further verifying the inhibitory roles of Fe^{3+}-EDTA complex in the PC/Fe^{3+}/PS system. These results evidenced that Fe^{3+}/Fe^{2+} cycle played the vital role in PC400/Fe^{3+}/PS system but not for the PC700/Fe^{3+}/PS system, in which the coupled PC700/PS might dominate the SMX removal.

To further investigate the role of Fe^{3+}/Fe^{2+} cycle in SMX removal, PC400 and PC700 were employed to the Fe^{2+}/PS system. PC400 remarkably boosted the SMX removal, and the removal efficiency of the PC400/Fe^{2+}/PS system was significantly higher than that of the Fe^{2+}/PS system (100 % vs 76.4 %) (Fig. 2e). However, PC700 only slightly accelerated the SMX removal in the PC700/Fe^{2+}/PS system than that of Fe^{2+}/PS system (81.7 % vs 76.4 %). These results verified the higher Fe^{3+}/Fe^{2+} cycle with the presence of PC400 than PC700. Besides, the SMX sorption was limited estimated by extraction after the reaction in different systems (Fig. S10), further indicated that the oxidation primarily contributed to the removal process.

3.3. Identification of reactive species

3.3.1. Radicals

To explore the roles of reactive species, selectively scavenging tests were performed in PC400/Fe^{3+}/PS and PC700/Fe^{3+}/PS systems. Ethanol is a scavenger for sulfate ($SO_4^{\bullet-}$) and hydroxyl ($^{\bullet}OH$) radicals [32]. Here, the addition of ethanol at the molar concentration of 1000 times of PS severely inhibited SMX degradation by 62.3 % in the PC400/Fe^{3+}/PS system (Fig. 3a). However, the same dose of ethanol only partially inhibited the SMX degradation by 29.3 % in the PC700/Fe^{3+}/PS system (Fig. 3b). Since ethanol could also quench nonradical ROS such as Fe(IV), the contribution of free radicals might be magnified by the quenching test [40], especially for PC400/Fe^{3+}/PS system, in which Fe(IV) played crucial roles and was detailedly discussed in Section 3.3.2. Besides, phenol addition severely inhibited the SMX degradation by 74.7 % in the PC400/Fe^{3+}/PS and by 42.9 % in PC700/Fe^{3+}/PS systems, respectively, which was higher than ethanol quencher (Fig. 3a-b), verifying the co-existing radical and nonradical reaction pathway.

EPR results showed that strong DMPO/$^{\bullet}OH$ adduct (four lines, 1:2:2:1) was clearly observed in both PC400/Fe^{3+}/PS and PC700/Fe^{3+}/PS systems (Fig. S11). The unseen DMPO/$SO_4^{\bullet-}$ adduct might be due to the quick transformation from DMPO/$SO_4^{\bullet-}$ adduct to DMPO/$^{\bullet}OH$ adduct [41]. The signal of DMPO/$^{\bullet}OH$ adduct in the PC400/Fe^{3+}/PS system was higher than that of the PC700/Fe^{3+}/PS system (Fig. S11), because DMPO/$^{\bullet}OH$ adducts might form via the direct oxidation of DMPO by generated Fe(IV), which was detailedly discussed later.

3.3.2. Nonradical species

To identify the possible generation of Fe(IV), PMSO was used as the probe compound since Fe(IV) could transform PMSO to $PMSO_2$, which was different from the radical-induced products [27]. PC400 or PC700 alone could remove about 8.68–16.0 μmol L^{-1} of PMSO (Fig. 3c). In the PC400/Fe^{3+}/PS system, the depletion of PMSO was 100 μmol L^{-1} and production of $PMSO_2$ was 46.4 μmol L^{-1}, whereas the production of $PMSO_2$ in the PC700/Fe^{3+}/PS system was 4.62 μmol L^{-1}, which was much lower than that of PC400/Fe^{3+}/PS system (Fig. 3c-d and Fig. S12). The results indicated the involvement of Fe(IV) in the PC400/Fe^{3+}/PS system; however, the contribution of Fe(IV) was insignificant in the PC700/Fe^{3+}/PS system.

Mössbauer experiment was conducted to further examine the existence of Fe(IV). In the PC400/Fe^{3+}/PS system, the identified Fe(IV) signal with the parameter isomer shift of -0.09 mm s^{-1} was observed in Fig. 3e [34,42,43], and the proportion of Fe(IV) reached 11.2 %. In contrast, no clear signal of Fe(IV) was found in the PC700/Fe^{3+}/PS system (Fig. 3f and Table S2). These results demonstrated that Fe(IV) existed in the PC400/Fe^{3+}/PS system while no Fe(IV) was found in the PC700/Fe^{3+}/PS system.

Besides, considering the possible singlet oxygen ($^1O_2$) generated in the PC400/Fe^{3+}/PS and PC700/Fe^{3+}/PS systems, FFA quenching experiment was performed. Results showed that FFA addition could not obviously inhibit the SMX removal in these two systems (Fig. S13), suggesting that $^1O_2$ was not the primary ROS. To further verify other nonradical pathways such as surface electron transfer, Linear Sweep Voltammetry measurement was performed. Result showed the synergistic increase of current in the co-presence of PS and SMX via the conductive bridge of PC700 in the PC700/PS system (Fig. S14). Specifically, electron migrates from the electron-donor of SMX to the acceptor of PC700/PS complexes (e.g., PC700-PS*) through the conductive bridge of PC700. However, the current could not be strengthened with the addition of both PS and SMX in the PC400/PS system. These results demonstrated that surface-confined electron transfer existed in the PC700/PS system instead of the PC400/PS system. Since PC700/PS system dominated the SMX removal in the PC700/Fe^{3+}/PS system, the surface electron transfer as the nonradical reaction pathway might exist in the PC700/Fe^{3+}/PS system.

3.3.3. Kinetics calculation

To distinguish the relative contributions of $SO_4^{\bullet-}$, $^{\bullet}OH$, and nonradical pathways for SMX degradation, competition kinetics test was conducted based on the reported method [28]. Briefly, degradation removal of the mixed system containing SMX, Nitrobenzene (NB), and Benzoic acid (BA) by the PC400/Fe^{3+}/PS and PC700/Fe^{3+}/PS systems were investigated. With the experimentally determined rate constants (k_{obs}) (Fig. S15) along with literature-reported second order rate constants of radicals toward the three probe compounds (Table S3), the steady-state concentrations of two radicals (e.g., $^{\bullet}OH$ and $SO_4^{\bullet-}$) were calculated based on the equations in Text S5. In the PC400/Fe^{3+}/PS system, the steady-state concentrations of $^{\bullet}OH$ and $SO_4^{\bullet-}$ were calculated to be 0.85 × 10^{-14} M and 3.51 × 10^{-14} M, respectively; in the

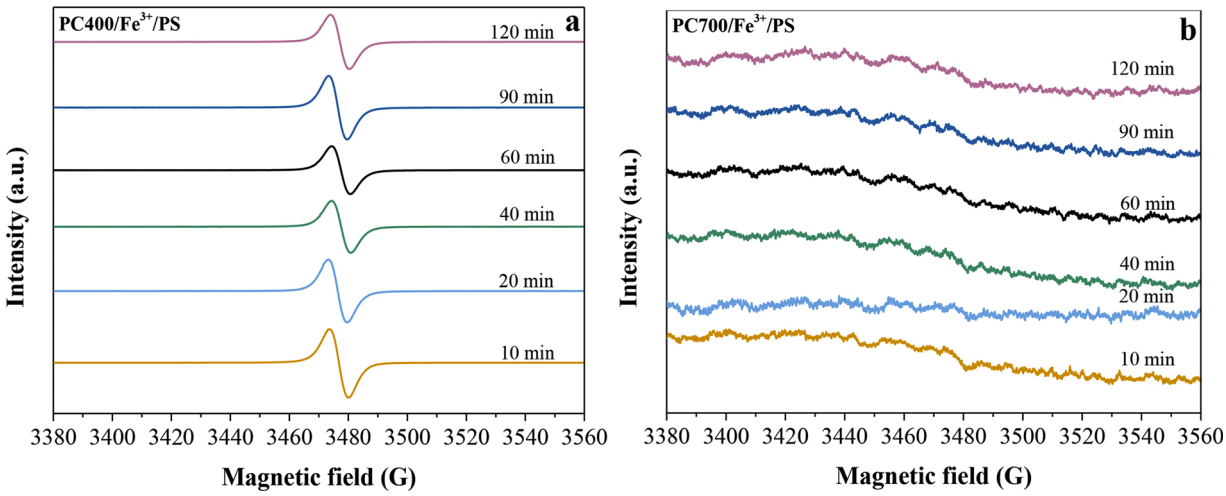

Fig. 4. Changes of PFRs on pyrolytic carbon during the PC400/Fe^{3+}/PS and PC700/Fe^{3+}/PS systems.

PC700/Fe^{3+}/PS system, the steady-state concentrations of $^{\bullet}OH$ and $SO_4^{\bullet-}$ were calculated to be 1.28×10^{-14} M and 1.09×10^{-14} M, respectively. Thus, the relative contribution of $^{\bullet}OH$, $SO_4^{\bullet-}$, and nonradical reactive species in the PC400/Fe^{3+}/PS system were estimated to be 28.8 %, 16.3 %, and 54.9 %, demonstrating the dominant role of nonradical oxidation pathway. In the PC700/Fe^{3+}/PS system, the relative contribution of nonradical pathway was 51.5 %, which was higher than that of $^{\bullet}OH$ and $SO_4^{\bullet-}$ oxidation pathway. These two systems both demonstrated that nonradical pathways had more significant contributions than radical oxidation pathways. The abovementioned results indicated that Fe(IV) mainly contributed to SMX degradation in the PC400/Fe^{3+}/PS system, whereas surface electron transfer might be the main reaction pathway in the PC700/Fe^{3+}/PS system.

3.4. Reaction mechanism

As mentioned above, PC400 exhibited excellent capacity to facilitate the Fe^{3+}/Fe^{2+} circulation, accelerating the continuous SMX degradation. In contrast, PC700 attained limited Fe^{3+}/Fe^{2+} cycles, leading to the non-continuous degradation. PC400 had high electron donating capacity as well as low graphitization degree and surface area (19.8 $m^2\ g^{-1}$), while PC700 possessed low electron donating capacity as well as the high graphitization degree and surface area (283 $m^2\ g^{-1}$) (Table S1). These different characteristics might contribute to the distinct catalytic performance of PCs for SMX degradation. The amounts of phenolic O—H groups were related with the electron donating capability [24]. In the PC400/Fe^{3+}/PS system, when PC400 reacted with Fe^{3+}, Fe^{3+} was reduced to Fe^{2+}; meanwhile, the phenolic O—H group in PC400 would be transformed to a semiquinone radical (Eq. (3)) [44,45]. Subsequently, semiquinone radicals as the intermediate in PC400 would react with Fe^{3+} to form quinones (Eq. (4)) [46]. Moreover, quinones would react with reactive species such as radicals to generate semiquinone radicals (Eq. (5)), which would again reduce Fe^{3+} to regenerate quinones and Fe^{2+} [45,47]. The above mechanism was verified by EPR analysis (Fig. 4a and Fig. S16). For the PC400/Fe^{3+}/PS system, EPR signal with a g factor of 2.0032 for semiquinone radical [48], decreased in first 60 min, then the signal increased as time prolonged to 90 min, and finally decreased at 120 min (Fig. 4a and Fig. S16), showing that the contents of semiquinone radical firstly decreased and then increased, and again decreased, further demonstrating the transformation between semiquinone radical and quinones. Then Fe^{2+} reacted with PS to generate Fe(IV) or radicals (Eqs. (1) and (6)). It was noted that the generated Fe(IV) was a transient species [34,49], and it would transform into Fe^{3+} (Eqs. (7) and (8)). These results could explain the reason for long-lasting Fe^{2+} generation, which could lead to the continuous degradation of SMX in PC400/Fe^{3+}/PS system.

However, in the PC700/Fe^{3+}/PS system, signals of semiquinone radical on PC700 were not observed (Fig. 4b), which implied that the redox processes of oxygen groups (e.g., phenolic O—H and quinones) were limited. Instead of functional groups, active sites associated with aromatic structure and high surface area might be the key factors for the surface electron-transfer mechanism [24]. It was liable to be deactivated after the repeated use due to the hindered interaction between PC700 and PS, thereby inhibiting the degradation. The catalytic mechanism of PC700 referred to the equations (Eqs. (9)–(13)).

The TOC result showed that both the PC400/Fe^{3+}/PS and PC700/Fe^{3+}/PS systems had good mineralization degree on SMX with TOC removal rate of 60.8 %–64.8 % (Fig. S17). To further explore the degradation mechanism, degradation products of SMX were detected. Based on the identified products (Fig. S18-S19 and Table S4) from the PC400/Fe^{3+}/PS system, hydroxylation and N—S bond cleavage of SMX molecule existed. However, in the PC700/Fe^{3+}/PS systems, isoxazole ring opening was observed, further demonstrating that the degradation mechanisms for the two systems were different. The possible degradation pathway of SMX in the PC400/Fe^{3+}/PS and PC700/Fe^{3+}/PS was drawn as shown in Fig. S20.

For PC400:

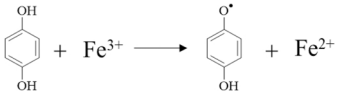

(3)

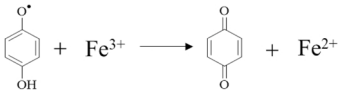

(4)

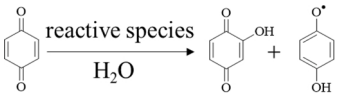

(5)

$$Fe^{2+} + S_2O_8^{2-} + H_2O \rightarrow Fe^{IV}O^{2+} + 2SO_4^{2-} + 2H^+ \quad (6)$$

$$Fe^{IV}O^{2+} + H^+ \rightarrow Fe^{3+} + \frac{1}{4}O_2 + \frac{1}{2}H_2O \quad (7)$$

$$Fe^{IV}O^{2+} + Fe^{2+} + 2H^+ \rightarrow 2Fe^{3+} + H_2O \quad (8)$$

For PC700:

$$PC700 + S_2O_8^{2-} \rightarrow PC700_{OX} + SO_4^{\bullet-} + SO_4^{2-} \quad (9)$$

$$SMX + PC700 + S_2O_8^{2-} \rightarrow SMX_{OX} + PC700 + 2SO_4^{2-} \quad (10)$$

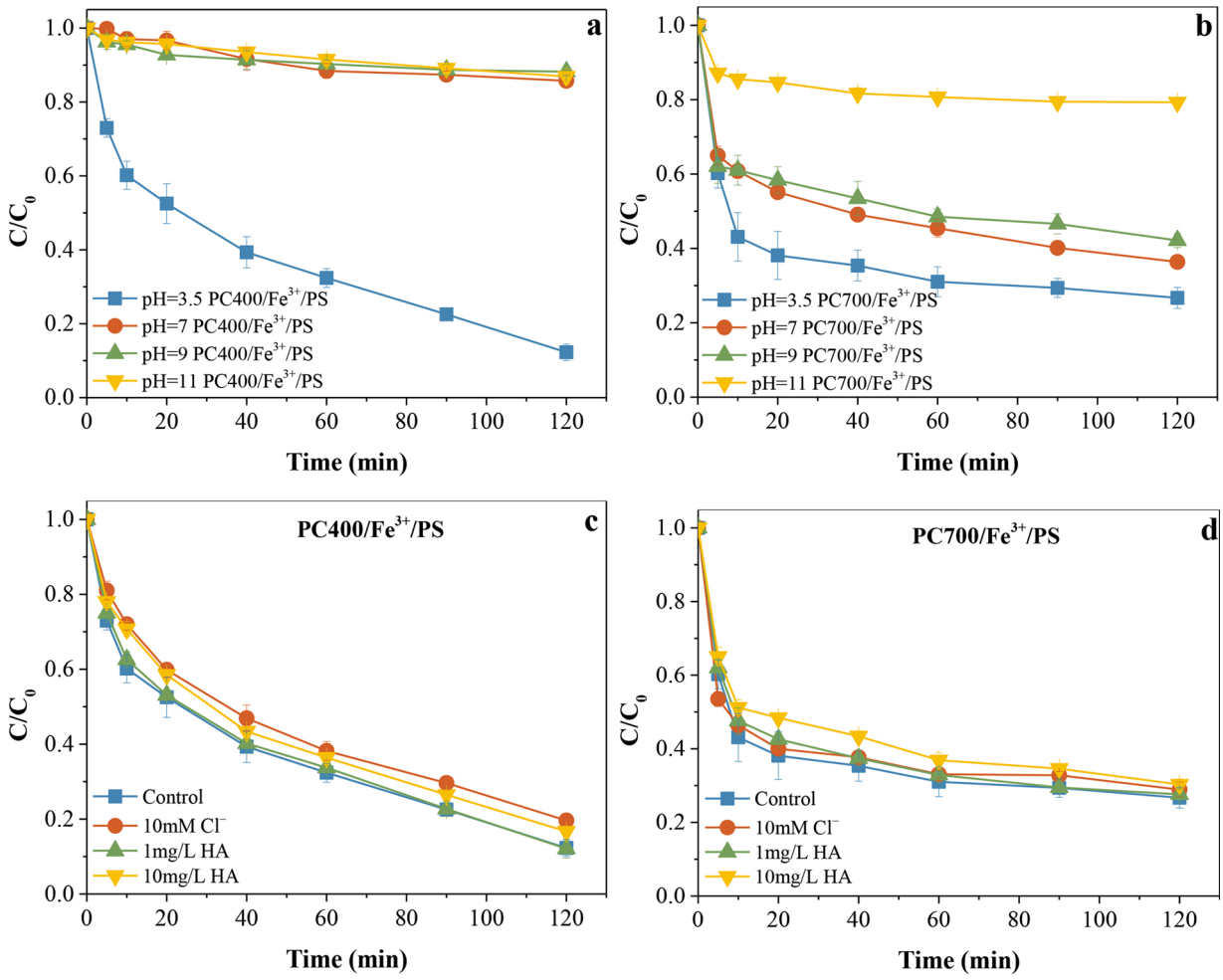

Fig. 5. Effect of pH value on the SMX removal in the PC400/Fe^{3+}/PS (a) and PC700/Fe^{3+}/PS (b) systems; effect of Cl^- and HA on SMX removal in the PC400/Fe^{3+}/PS (c) and PC700/Fe^{3+}/PS (d) systems. Reaction conditions: PS: 2 mmol L^{-1}, PC400 or PC700: 0.5 g L^{-1}, Fe^{3+}: 1 mmol L^{-1}, (a-b) SMX: 10 mg L^{-1}, pH = 3.5/7/9/11, (c-d) Cl^-: 10 mmol L^{-1}, HA: 1 and 10 mg L^{-1}, SMX: 10 mg L^{-1}, pH = 3.5.

$$SO_4^{\bullet-} + H_2O \rightarrow SO_4^{2-} + \bullet OH + H^+ \quad (11)$$

$$SO_4^{\bullet-} + OH^- \rightarrow SO_4^{2-} + \bullet OH \quad (12)$$

$$SO_4^{\bullet-} / \bullet OH + SMX \rightarrow SMX_{OX} \quad (13)$$

3.5. *Influence of environmental factors and application potential in real water*

Influences of environmental factors on SMX degradation were investigated, including initial solution pH (unbuffered), chloride, and humic acid (HA) (Fig. 5a-d). The PC400/Fe^{3+}/PS system was sensitive to the solution pH, and SMX degradation was obviously inhibited by 73.4 %–75.9 % at pH 7/9/11 compared to the efficiency at pH 3.5 (Fig. 5a). In the PC400/Fe^{3+}/PS system, the final solution pH value was 6.20, 7.43, and 10.6 whereas the initial solution pH was 7, 9, and 11, respectively (Fig. S21). Fe^{3+} would be transformed into oxyhydroxides at pH $\geq$ 5.4 via precipitation reactions [10,50], which might be the reason for significantly retarded SMX degradation in the PC400/Fe^{3+}/PS system. Additionally, our previous study reported that pyrolytic carbons derived from low-temperature pyrolysis possessed better reducing ability at pH 2 than that at pH 4 because that the reduction process was a proton-consuming reaction and the increase of pH would result in the depletion of protons [21]. On this basis, PC400 at pH 3.5 would release more electrons to the acceptor (Fe^{3+}) to generate more Fe^{2+} than that at pH 7/9/11, thereby resulting in more SMX degradation. These two reasons collectively resulted in the hindered SMX degradation in the PC400/Fe^{3+}/PS system as the pH increased from 3.5–7/9/11. However, in the PC700/Fe^{3+}/PS system, SMX degradation was only inhibited by 9.66 %–15.4 % at pH 7/9 compared to the efficiency at pH 3.5, while SMX degradation was significantly inhibited at pH 11 (Fig. 5b). On one hand, Fe^{3+} was hardly to form oxyhydroxides in the PC700/Fe^{3+}/PS system at initial pH 7/9, because pH gradually decreased to 3.80 and 5.18 along with the reaction while oxyhydroxides was formed at initial pH 11 due to the high final pH of 10.4 (Fig. S21). On the other hand, PC700/PS system dominated the SMX removal in the PC700/Fe^{3+}/PS system, PC700 at pH 10.4 had more surface negative charge compared to that at pH 3.80/5.18 (Fig. S8), which might affect the formation of PC700-PS* and thereby inhibiting the SMX degradation. The above explanations together contributed to the much less influenced SMX degradation in the PC700/Fe^{3+}/PS system as the pH increased from 3.5–7/9, compared to that at pH 11.

The presence of 10 mM chloride ions slightly inhibited 7.34 % of SMX degradation in the PC400/Fe^{3+}/PS system, and negligible effect of chloride was observed in the PC700/Fe^{3+}/PS system (Fig. 5c-d). The reduced SMX removal was ascribed to the fact that chloride ion could easily scavenge free radicals to produce less reactive chlorine radicals [51]. However, the reduced removal was limited, further exhibiting that reactive species in the two systems was prior to react with SMX regardless of co-existing inorganic substrates (e.g., chloride). The presence of HA (e.g., 1 and 10 mg L^{-1}) possessed a marginal effect on SMX

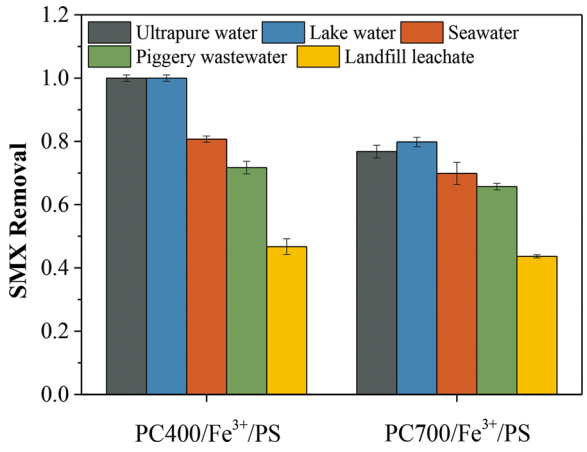

Fig. 6. SMX removal in real water matrixes in the PC400/Fe^{3+}/PS and PC700/Fe^{3+}/PS systems. Reaction conditions: SMX: 10 mg L^{-1}, PS: 2 mmol L^{-1}, PC400 or PC700: 0.5 g L^{-1}, Fe^{3+}: 1 mmol L^{-1}, pH = 3.5, T = 12 h, and temperature: 25 °C; real water matrixes: lake water, seawater, piggery wastewater, and landfill leachate.

degradation by 4.44 % and 3.60 % inhibition in the PC400/Fe^{3+}/PS and PC700/Fe^{3+}/PS systems, respectively (Fig. 5c-d). The limited effect of chloride ions and HA implied the vital roles of nonradical reaction pathway (e.g., Fe(IV) and surface electron transfer).

The PC400/Fe^{3+}/PS and PC700/Fe^{3+}/PS systems were applied in the real water, including lake water, seawater, piggery wastewater, and landfill leachate (Fig. 6). Compared to ultrapure water, SMX removal was barely affected in lake water in both PC400/Fe^{3+}/PS and PC700/Fe^{3+}/PS systems. Regardless of the high concentration of Cl^- in seawater (Cl^-: 7286 mg L^{-1}), 80.7 % and 69.9 % of SMX removal was still obtained in the PC400/Fe^{3+}/PS system and PC700/Fe^{3+}/PS system, respectively (Fig. 6 and Table 1), which indicated the merits of nonradical pathway. Although components in piggery wastewater (TOC: 821 mg L^{-1}; Cl^-: 418.1 mg L^{-1}) and landfill leachate (TOC: 1389 mg L^{-1}; Cl^-: 4479 mg L^{-1}) were complex, SMX removal efficiency was still appreciable in the PC400/Fe^{3+}/PS (46.7 %–71.7 %) and PC700/Fe^{3+}/PS (43.6 %–65.7 %) system. The appreciable removal could be achieved at the low contents of PC400/PC700 and PS (PC400 or PC700: 0.5 g L^{-1}, PS: 2 mmol L^{-1}). Thus, the nonradical systems were applicable in the real water systems.

4. Conclusion

Pyrolytic carbons (PC) enhanced the oxidation capability of Fe^{3+}/PS systems for the SMX degradation. Pyrolytic carbon upon low-temperature possessed the high Fe^{3+}/Fe^{2+} cycle due to the regenerated semiquinone radical, which resulted in the continuous SMX degradation. However, pyrolytic carbon upon high-temperature could not maintain the ongoing SMX degradation. Moreover, the appreciable SMX removal was obtained in the real water systems by the PC/Fe^{3+}/PS system through the Fe(IV) and surface electron transfer depended nonradical pathways. Compared to traditional Fe^{2+}/PS system, PC/Fe^{3+}/PS coupled system showed the great potential for practical application because of the advantages of facile synthesis, low cost, great redox ability, high conductivity and stability. The proposed mechanism would help understand the structure-application relationships in carbon-based persulfate systems. Future work is encouraged to investigate the pyrolytic carbons derived from a diversity of bio-feedstocks for environmental applications such as Fenton-like systems.

CRediT authorship contribution statement

Jun Liang: Conceptualization, Methodology, Experiments, Writing - Original Draft. **Xiaoguang Duan:** Supervision, Reviewing, Conceptualization, Writing and Editing. **Xiaoyun Xu:** Supervision, Reviewing, Methodology, Conceptualization, Writing and Editing, Funding acquisition. **Kexin Chen**, **Fei Wu:** Methodology, Formal analysis. **Hao Qiu**, **Chengshuai Liu**, **Shaobin Wang:** Supervision, Reviewing. **Xinde Cao:** Supervision, Reviewing, Conceptualization, Writing and Editing, Funding acquisition.

Declaration of Competing Interest

The authors declare that they have no known competing financial interests or personal relationships that could have appeared to influence the work reported in this paper.

Acknowledgements

This work was supported in part by National Natural Science Foundation of China (No. 21537002, 21777095, 42077112), National Key R&D Program of China (No. 2018YFC1802700, 2018YFC1800600), Science and Technology Commission of Shanghai Municipality (No. 20ZR1429100).

Appendix A. Supplementary data

Supplementary material related to this article can be found, in the online version, at doi:https://doi.org/10.1016/j.apcatb.2021.120446.

References

[1] E. Neyens, J. Baeyens, A review of classic Fenton's peroxidation as an advanced oxidation technique, J. Hazard. Mater. 98 (2003) 33–50.
[2] S. Wacławek, H.V. Lutze, K. Grübel, V.V.T. Padil, M. Černík, D.D. Dionysiou, Chemistry of persulfates in water and wastewater treatment: a review, Chem. Eng. J. 330 (2017) 44–62.
[3] P. Devi, U. Das, A.K. Dalai, In-situ chemical oxidation: principle and applications of peroxide and persulfate treatments in wastewater systems, Sci. Total Environ. 571 (2016) 643–657.
[4] S.Y. Oh, H.W. Kim, J.M. Park, H.S. Park, C. Yoon, Oxidation of polyvinyl alcohol by persulfate activated with heat, Fe^{2+}, and zero-valent iron, J. Hazard. Mater. 168 (2009) 346–351.
[5] W.D. Oh, T.T. Lim, Design and application of heterogeneous catalysts as peroxydisulfate activator for organics removal: an overview, Chem. Eng. J. 358 (2019) 110–133.
[6] L. Chen, J. Ma, X. Li, J. Zhang, J. Fang, Y. Guan, P. Xie, Strong enhancement on Fenton oxidation by addition of hydroxylamine to accelerate the ferric and ferrous iron cycles, Environ. Sci. Technol. 45 (2011) 3925–3930.
[7] Y.T. Lin, C. Liang, C.W. Yu, Trichloroethylene degradation by various forms of iron activated persulfate oxidation with or without the assistance of ascorbic acid, Ind. Eng. Chem. Res. 55 (2016) 2302–2308.
[8] J. Zou, J. Ma, L. Chen, X. Li, Y. Guan, P. Xie, C. Pan, Rapid acceleration of ferrous iron/peroxymonosulfate oxidation of organic pollutants by promoting Fe(III)/Fe (II) cycle with hydroxylamine, Environ. Sci. Technol. 47 (2013) 11685–11691.
[9] M. Xing, W. Xu, C. Dong, Y. Bai, J. Zeng, Y. Zhou, J. Zhang, Y. Yin, Metal sulfides as excellent co-catalysts for H_2O_2 decomposition in advanced oxidation processes, Chem 4 (2018) 1359–1372.
[10] P. Zhou, W. Ren, G. Nie, X. Li, X. Duan, Y. Zhang, S. Wang, Fast and long-lasting Iron(III) reduction by boron toward green and accelerated Fenton chemistry, Angew. Chem. Int. Ed. 59 (2020) 16517–16526.
[11] C. Liang, C.J. Bruell, M.C. Marley, K.L. Sperry, Persulfate oxidation for in situ remediation of TCE. II. activated by chelated ferrous ion, Chemosphere 55 (2004) 1225–1233.
[12] L. Zhu, J. Ji, J. Liu, S. Mine, M. Matsuoka, J. Zhang, M. Xing, Designing 3D-MoS_2 sponge as excellent cocatalysts in advanced oxidation processes for pollutant control, Angew. Chem. Int. Ed. 59 (2020) 13968–13976.
[13] J. Li, Y. Wan, Y. Li, G. Yao, B. Lai, Surface Fe(III)/Fe(II) cycle promoted the degradation of atrazine by peroxymonosulfate activation in the presence of hydroxylamine, Appl. Catal. B: Environ. 256 (2019), 117782.
[14] H. Zhou, H. Zhang, Y. He, B. Huang, C. Zhou, G. Yao, B. Lai, Critical review of reductant-enhanced peroxide activation processes: trade-off between accelerated Fe^{3+}/Fe^{2+} cycle and quenching reactions, Appl. Catal. B: Environ. 286 (2021), 119900.
[15] Y. Ji, C. Ferronato, A. Salvador, X. Yang, J.M. Chovelon, Degradation of ciprofloxacin and sulfamethoxazole by ferrous-activated persulfate: implications for remediation of groundwater contaminated by antibiotics, Sci. Total Environ. 472 (2014) 800–808.

[16] T. Li, Z. Zhao, Q. Wang, P. Xie, J. Ma, Strongly enhanced Fenton degradation of organic pollutants by cysteine: an aliphatic amino acid accelerator outweighs hydroquinone analogues, Water Res. 105 (2016) 479–486.
[17] H. Meng, C. Nie, W. Li, X. Duan, B. Lai, Z. Ao, S. Wang, T. An, Insight into the effect of lignocellulosic biomass source on the performance of biochar as persulfate activator for aqueous organic pollutants remediation: epicarp and mesocarp of citrus peels as examples, J. Hazard. Mater. 399 (2020), 123043.
[18] W. Liu, C. Nie, W. Li, Z. Ao, S. Wang, T. An, Oily sludge derived carbons as peroxymonosulfate activators for removing aqueous organic pollutants: performances and the key role of carbonyl groups in electron-transfer mechanism, J. Hazard. Mater. 414 (2021), 125552.
[19] P. Zhou, J. Zhang, Z. Xiong, Y. Liu, X. Huo, X. Cheng, W. Li, F. Cheng, Y. Zhang, C_{60} fullerol promoted Fe(III)/H_2O_2 Fenton oxidation: role of photosensitive Fe(III)-fullerol complex, Appl. Catal. B: Environ. 265 (2020), 118264.
[20] Z. Yang, A. Yu, C. Shan, G. Gao, B. Pan, Enhanced Fe(III)-mediated Fenton oxidation of atrazine in the presence of functionalized multi-walled carbon nanotubes, Water Res. 137 (2018) 37–46.
[21] X. Xu, H. Huang, Y. Zhang, Z. Xu, X. Cao, Biochar as both electron donor and electron shuttle for the reduction transformation of Cr(VI) during its sorption, Environ. Pollut. 244 (2019) 423–430.
[22] Y. Qin, G. Li, Y. Gao, L. Zhang, Y.S. Ok, T. An, Persistent free radicals in carbon-based materials on transformation of refractory organic contaminants (ROCs) in water: a critical review, Water Res. 137 (2018) 130–143.
[23] Z. Xu, X. Xu, X. Tao, C. Yao, D.C.W. Tsang, X. Cao, Interaction with low molecular weight organic acids affects the electron shuttling of biochar for Cr(VI) reduction, J. Hazard. Mater. 378 (2019), 120705.
[24] Z. Xu, X. Xu, Y. Zhang, Y. Yu, X. Cao, Pyrolysis-temperature depended electron donating and mediating mechanisms of biochar for Cr(VI) reduction, J. Hazard. Mater. 388 (2020), 121794.
[25] Y.D. Chen, R. Wang, X. Duan, S. Wang, N.Q. Ren, S.H. Ho, Production, properties, and catalytic applications of sludge derived biochar for environmental remediation, Water Res. 187 (2020), 116390.
[26] W. Ren, L. Xiong, X. Yuan, Z. Yu, H. Zhang, X. Duan, S. Wang, Activation of peroxydisulfate on carbon nanotubes: electron-transfer mechanism, Environ. Sci. Technol. 53 (2019) 14595–14603.
[27] Z. Wang, J. Jiang, S. Pang, Y. Zhou, C. Guan, Y. Gao, J. Li, Y. Yang, W. Qiu, C. Jiang, Is sulfate radical really generated from peroxydisulfate activated by Iron (II) for environmental decontamination? Environ. Sci. Technol. 52 (2018) 11276–11284.
[28] H. Dong, Y. Li, S. Wang, W. Liu, G. Zhou, Y. Xie, X. Guan, Both Fe(IV) and radicals are active oxidants in the Fe(II)/peroxydisulfate process, Environ. Sci. Technol. Lett. 7 (2020) 219–224.
[29] X. Cao, W. Harris, Properties of dairy-manure-derived biochar pertinent to its potential use in remediation, Bioresour. Technol. 101 (2010) 5222–5228.
[30] L. Zhao, W. Zheng, X. Cao, Distribution and evolution of organic matter phases during biochar formation and their importance in carbon loss and pore structure, Chem. Eng. J. 250 (2014) 240–247.
[31] J. Liang, X. Xu, W. Qamar Zaman, X. Hu, L. Zhao, H. Qiu, X. Cao, Different mechanisms between biochar and activated carbon for the persulfate catalytic degradation of sulfamethoxazole: roles of radicals in solution or solid phase, Chem. Eng. J. 375 (2019), 121908.
[32] G.P. Anipsitakis, D.D. Dionysiou, Radical generation by the interaction of transition metals with common oxidants, Environ. Sci. Technol. 38 (2004) 3705–3712.
[33] E.T. Yun, H.Y. Yoo, H. Bae, H.I. Kim, J. Lee, Exploring the role of persulfate in the activation process: radical precursor versus electron acceptor, Environ. Sci. Technol. 51 (2017) 10090–10099.
[34] S. Liang, L. Zhu, J. Hua, W. Duan, P.T. Yang, S.L. Wang, C. Wei, C. Liu, C. Feng, Fe^{2+}/HClO reaction produces $Fe^{IV}O^{2+}$: an enhanced advanced oxidation process, Environ. Sci. Technol. 54 (2020) 6406–6414.
[35] D. He, J. Ma, R.N. Collins, T.D. Waite, Effect of structural transformation of nanoparticulate zero-valent iron on generation of reactive oxygen species, Environ. Sci. Technol. 50 (2016) 3820–3828.
[36] S.H. Ho, Y.D. Chen, R. Li, C. Zhang, Y. Ge, G. Cao, M. Ma, X. Duan, S. Wang, N. Q. Ren, N-doped graphitic biochars from C-phycocyanin extracted *Spirulina* residue for catalytic persulfate activation toward nonradical disinfection and organic oxidation, Water Res. 159 (2019) 77–86.
[37] A.M. Jones, P.J. Griffin, T.D. Waite, Ferrous iron oxidation by molecular oxygen under acidic conditions: the effect of citrate, EDTA and fulvic acid, Geochim. Cosmochim. Acta 160 (2015) 117–131.
[38] T. Hirokawa, K. Nishimoto, Y. Jie, K. Ito, F. Nishiyama, N. Ikuta, S. Hayakawa, Isotachophoretic separation behavior of rare-earth EDTA chelates and analysis of minor rare-earth elements in an iron ore by bidirectional isotachophoresis–particle-induced X-ray emission, J. Chromatogr. A 919 (2001) 417–426.
[39] Y. Zhang, M. Zhou, A critical review of the application of chelating agents to enable Fenton and Fenton-like reactions at high pH values, J. Hazard. Mater. 362 (2019) 436–450.
[40] O. Pestovsky, A. Bakac, Reactivity of aqueous Fe(IV) in hydride and hydrogen atom transfer reactions, J. Am. Chem. Soc. 126 (2004) 13757–13764.
[41] G.S. Timmins, K.J. Liu, E.J.H. Bechara, Y. Kotake, H.M. Swartz, Trapping of free radicals with direct in vivo EPR detection: a comparison of 5,5-dimethyl-1-pyrroline-N-oxide and 5-diethoxyphosphoryl-5-methyl-1-pyrroline-N-oxide as spin traps for HO and $SO_4^{\bullet-}$, Free Radic. Biol. Med. 27 (1999) 329–333.
[42] P. Novak, M. Kolar, L. Machala, K.M. Siskova, F. Karlicky, M. Petr, R. Zboril, Transformations of ferrates(iv,v,vi) in liquids: mössbauer spectroscopy of frozen solutions, Phys. Chem. Chem. Phys. 20 (2018) 30247–30256.
[43] J.Y.C. Chen, L. Dang, H. Liang, W. Bi, J.B. Gerken, S. Jin, E.E. Alp, S.S. Stahl, Operando analysis of NiFe and Fe oxyhydroxide electrocatalysts for water oxidation: detection of Fe^{4+} by Mössbauer spectroscopy, J. Am. Chem. Soc. 137 (2015) 15090–15093.
[44] G. Fang, J. Gao, D.D. Dionysiou, C. Liu, D. Zhou, Activation of persulfate by quinones: free radical reactions and implication for the degradation of PCBs, Environ. Sci. Technol. 47 (2013) 4605–4611.
[45] Y. Wang, T. Pan, Y. Yu, Y. Wu, Y. Pan, X. Yang, A novel peroxymonosulfate (PMS)-enhanced iron coagulation process for simultaneous removal of trace organic pollutants in water, Water Res. 185 (2020), 116136.
[46] C.K. Duesterberg, T.D. Waite, Kinetic modeling of the oxidation of p-Hydroxybenzoic acid by Fenton's reagent: implications of the role of quinones in the redox cycling of iron, Environ. Sci. Technol. 41 (2007) 4103–4110.
[47] M. Nien Schuchmann, E. Bothe, J. von Sonntag, C. von Sonntag, Reaction of OH radicals with benzoquinone in aqueous solutions. A pulse radiolysis study, J. Chem. Soc. Perkin Trans. I 2 (1998) 791–796.
[48] K. Zhang, P. Sun, M.C.A.S. Faye, Y. Zhang, Characterization of biochar derived from rice husks and its potential in chlorobenzene degradation, Carbon 130 (2018) 730–740.
[49] J. Zhu, F. Yu, J. Meng, B. Shao, H. Dong, W. Chu, T. Cao, G. Wei, H. Wang, X. Guan, Overlooked role of Fe(IV) and Fe(V) in organic contaminant oxidation by Fe(VI), Environ. Sci. Technol. 54 (2020) 9702–9710.
[50] A. Stefánsson, Iron(III) hydrolysis and solubility at 25 °C, Environ. Sci. Technol. 41 (2007) 6117–6123.
[51] C. Liang, Z.S. Wang, N. Mohanty, Influences of carbonate and chloride ions on persulfate oxidation of trichloroethylene at 20 °C, Sci. Total Environ. 370 (2006) 271–277.